This article has been accepted for publication in a future issue of this journal, but has not been fully edited. Content may change prior to final publication. Citation information: DOI 10.1109/TII.2019.2900119, IEEE Transactions on Industrial Informatics

A Sensorless Hand Guiding Scheme Based on Model Identification and Control for Industrial Robot

Shaolin Zhang, Shuo Wang, Fengshui Jing, and Min Tan

***Abstract*—Most industrial robots are not capable of teaching by hand and require path points to be specified by teaching pendants. To enable the teaching of industrial robots by hand without any force sensors, this paper proposes a scheme to minimize the external force estimation error and reduce disturbance in the guiding task by using the virtual mass and virtual friction model. In this case, the maximum velocity and acceleration of the robot end-effector shall be limited to ensure safety. Thus, the operator is allowed to guide the robot by hand. The joint torque is obtained from the motor current. The inertial force and friction of the links and driving systems are analyzed. The nonlinear dynamic model of the industrial robot is built and its parameters are calibrated by a nonlinear method. The force estimation is referenced to set the virtual friction and design the force following controller. Hence the end-effector can follow the direction of external force compliantly and suppress jitters. Finally, several experiments on a six-degree-of-freedom industrial robot demonstrate the validity of the proposed control scheme.**

***Index Terms*—Industrial robot, dynamic model, parameter calibration, human-robot interaction, virtual friction.**

I. Introduction

MOST collaboration robots are lightweight manipulators with DC motors and force sensors, such as UR [1] and LBR iiwa [2]. However, in the field of stacking, welding, and spraying, most multi-joint industrial robots adopt AC servo systems and gearboxes with high reduction ratios. Further, they work with heavy loads and always have no force sensors or safety skins [3]. These robots move along a trajectory that is pre-programmed by teaching pendants for a given job. If they could detect external forces and follow the traction, the teaching task could be achieved by hand guiding. Then, these industrial robots could switch to another task quickly and become more adaptable to small batch production. Therefore, force detection and control for these types of industrial robots have great research value.

This paper focuses on a hand guiding control scheme for industrial robot teaching. The operator guides the robot end-effector to the desired pose by hand. The robot estimates the external force and generates a trajectory to follow it. Two components are added to the industrial robot control system for the hand guiding task: an external force estimator and a force following controller. Much research has been conducted on the external force measurement or estimation for multi-joint robots. It is easy to measure the external force using a six-dimensional force sensor installed on the robot end-effector [4]. However, these sensors are expensive and industrial robots usually do not have such sensors. Another method is to measure the joint torque and calculate the external force. [5] proposed a force estimator based on momentum conservation of the manipulator links. [6] proposed a similar method, but the external force was feedback based on the commanded control force by the computer. The motors work in torque mode. Thus, the external force can affect the motion of manipulator links directly, resulting in a change of momentum. However, the motors of industrial robots usually work in position mode and the controllers of standard configuration are forbidden to be modified. Moreover, most industrial robots do not provide the dynamic models needed in this method. Another method is to obtain the external force in each joint by subtracting the driving torque of manipulator links from the total torque provided by the motor [7] [8]. Some observers have been designed for the detection [9] [10]. These methods are based on the calibration of dynamic parameters. However, industrial robots usually do not have torque sensors and the driving torque is obtained from the motor current [11], which includes the inertial force and friction of the motor and gearbox. Because the motor inertia is large and the lubrication is not always good, ignoring the effects of the motor and gearbox will result in larger errors in the force estimation and lead to poor guiding performance.

To guide by hand, a force following controller is required for the robot control system. It allows a part of motion determined by the external force. [12] proposed a general framework of online planning a desired trajectory under physical limitations whose mathematical expression is unknown in advance. [13] developed an integrated control design for slave manipulators to handle a target object cooperatively under the control of master manipulators. The communication delays and nonlinearities existing in the environmental dynamics are analyzed. However, in addition to the online trajectory planning and interaction with the environment, the operability of the manipulator should be considered. One method is to adopt the closed-loop velocity control strategy and set the desired velocity to zero [6] [14]. The proportional parameters

This work was supported in part by the National Natural Science Foundation of China (U1713222, 61773378, 61421004, U1806204) and in part by the Youth Innovation Promotion Association CAS. Paper no. TII-18-2937. (Corresponding author: Shuo Wang.)

S. Zhang, S. Wang, F. Jing, and M. Tan are with the State Key Laboratory of Management and Control for Complex Systems, Institute of Automation, Chinese Academy of Sciences, Beijing 100190, China and also with the University of Chinese Academy of Sciences, Beijing 100049, China. S. Wang is also with the CAS Center for Excellence in Brain Science and Intelligence Technology, Shanghai 200031, China. (e-mail: zhangshaolin2015@ia.ac.cn; shuo.wang@ia.ac.cn; fengshui.jing@ia.ac.cn; min.tan@ia.ac.cn).

This article has been accepted for publication in a future issue of this journal, but has not been fully edited. Content may change prior to final publication. Citation information: DOI 10.1109/TII.2019.2900119, IEEE Transactions on Industrial Informatics

of the controller are adjusted to obtain an appropriate stiffness. The robot can be pushed forward by the external force and can decelerate and stop under the closed-loop control. In addition to proportional control, mass-spring-damping models [15] [16] and some other models [17] [18] can also be used. However, the resistance generated by the closed loop is not intuitive for hand guiding. There is no clear reference about how to set the parameters such as stiffness. It is difficult to guide a robot with excessive stiffness by hand, whereas too small a stiffness could result in a long time for deceleration. Moreover, the modeling uncertainties and measurement noises are not considered in these cases.

In this paper, an external force estimation method based on the dynamic model is proposed. The driving torque is obtained from the motor current. Since the measurement of driving torque is affected by the motor and gearbox, the friction and noise are larger than those of lightweight manipulators and make the robot difficult to guide by hand. Therefore, a model of the driving system is built in this study. The inertial force and friction parameters are calibrated by a nonlinear method. A force following controller is designed based on virtual mass and virtual friction. The external force pushes the end-effector forward and the virtual friction is a hypothetical resistance. The modeling uncertainties and measurement noises are estimated with the calibrated model. In the experiments, the angular position of each joint keeps stationary first. The end-effector moves if the external force applied to the robot is larger than the virtual friction. When the external force is removed, the end-effector decelerates until stopped.

The main contributions of this paper are as follows.

1) The nonlinear dynamic model of the driving system with consideration of motors and gearboxes is built for a six-degree-of-freedom industrial manipulator. The corresponding parameter calibration method is proposed. The external force estimation noise is calculated and discussed.
2) A force following controller based on virtual mass and virtual friction is presented for robot teaching. The influence of noise is analyzed.

The rest of this paper is organized as follows. First, we present the preliminaries in Section II. The hand guiding control scheme is introduced in Section III. The dynamic model and force following controller are designed. Finally, the experiments and discussions are described in Section IV and we conclude in Section V.

II. Preliminaries

Usually, robot manufacturers do not provide the dynamic model. A parameter calibration is required before external force estimation. In the descriptions throughout the text we adopted the following subscripts:

- m: variables related to the motor.
- g: variables related to the gearbox.
- ω: noise.
- f: friction.
- c: variables related to Coulomb friction.
- s: variables related to static friction.
- i: $i = 1..n$, where n is the number of links.
- k: variables in Cartesian space.
- j: variables in joint space.
- d: variables related to inertial force.
- ext: "external", exerted by the operator.
- $total$: driving torque of the motor.
- x, y, z: coordinate axes.

The dynamic equation of a multi-joint robot under external force can be described as

$$\boldsymbol{\tau}_d = \boldsymbol{\tau}_j + \boldsymbol{\tau}_{ext} \tag{1}$$

where $\boldsymbol{\tau}_d$ is the inertial force vector of robot links, $\boldsymbol{\tau}_j$ is the driving force vector, and $\boldsymbol{\tau}_{ext}$ is the external force applied to the robot links.

For a multi-joint serial robot, the inertial force of links can be described as [19]

$$\boldsymbol{\tau}_d = \boldsymbol{M}(\boldsymbol{q})\ddot{\boldsymbol{q}} + \boldsymbol{V}(\boldsymbol{q}, \dot{\boldsymbol{q}}) + \boldsymbol{G}(\boldsymbol{q}) \tag{2}$$

where $\boldsymbol{M}(\boldsymbol{q})$ is the inertia matrix of robot links, $\boldsymbol{V}(\boldsymbol{q}, \dot{\boldsymbol{q}})$ is the centrifugal and Coriolis forces, $\boldsymbol{G}(\boldsymbol{q})$ is the gravity vector, and $\boldsymbol{q}, \dot{\boldsymbol{q}}, \ddot{\boldsymbol{q}}$ are the angular position, angular velocity, and angular acceleration, respectively.

Equation (2) includes the kinematic and dynamic parameters. The kinematic parameters are assumed to be known. $\boldsymbol{q}$ is measured by angular position sensors, and $\dot{\boldsymbol{q}}, \ddot{\boldsymbol{q}}$ are observed by offline differentiation of $\boldsymbol{q}$. However, the dynamic parameters are unknown and need to be calibrated.

To calibrate the dynamic parameters, (2) can be expressed in a linear form of the parameters [20]:

$$\boldsymbol{\tau}_d = \boldsymbol{K}\boldsymbol{\phi} \tag{3}$$

where

$$\boldsymbol{\phi} = \begin{pmatrix} \boldsymbol{\phi}_1 \\ \cdot \\ \cdot \\ \boldsymbol{\phi}_n \end{pmatrix}$$

$$\boldsymbol{\phi}_i = \begin{pmatrix} \boldsymbol{m}_i \\ \boldsymbol{m}_i \boldsymbol{c}_i \\ \boldsymbol{l}(\bar{\boldsymbol{I}}_i) \end{pmatrix}$$

$$\boldsymbol{l}(\bar{\boldsymbol{I}}_i) = \begin{pmatrix} \bar{\boldsymbol{I}}_{i11} \\ \bar{\boldsymbol{I}}_{i12} \\ \bar{\boldsymbol{I}}_{i13} \\ \bar{\boldsymbol{I}}_{i22} \\ \bar{\boldsymbol{I}}_{i23} \\ \bar{\boldsymbol{I}}_{i33} \end{pmatrix}$$

$$\bar{\boldsymbol{I}}_i = \begin{pmatrix} \bar{I}_{i11} & \bar{I}_{i12} & \bar{I}_{i13} \\ \bar{I}_{i12} & \bar{I}_{i22} & \bar{I}_{i23} \\ \bar{I}_{i13} & \bar{I}_{i23} & \bar{I}_{i33} \end{pmatrix}, i = 1..n.$$

The matrix $\boldsymbol{K}$ is only related to the kinematic parameters. It is known when the angular position, angular velocity, and angular acceleration are given. $\boldsymbol{\phi}_i$ contains the dynamic parameters of joint i, including mass $\boldsymbol{m}_i$, centroid $\boldsymbol{c}_i$, and rotational inertia $\bar{\boldsymbol{I}}_i$. n is the number of links.

In addition to the model of links, the gearbox model is also needed in the case of current feedback. The friction of robot joints includes Coulomb friction, viscous friction, and

This article has been accepted for publication in a future issue of this journal, but has not been fully edited. Content may change prior to final publication. Citation information: DOI 10.1109/TII.2019.2900119, IEEE Transactions on Industrial Informatics

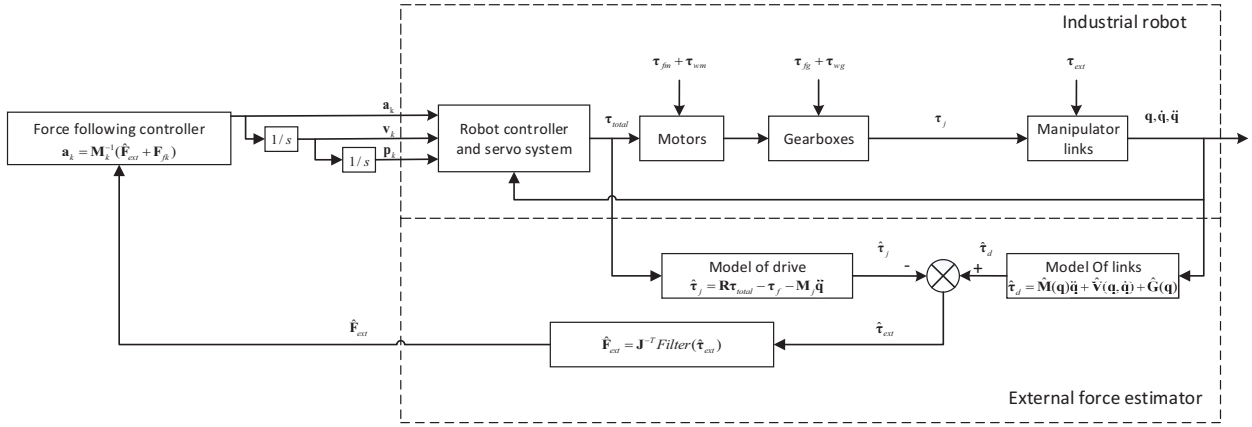

Fig. 1. The block diagram of sensorless hand guiding control scheme

static friction. The commonly used friction model is the LuGre friction model [21]. The friction torque τ_f is:

$$\tau_f = \left[F_c + (F_s - F_c)e^{-\left|\frac{\dot{q}}{\dot{q}_s}\right|^{\delta_s}}\right]\mathrm{sgn}(\dot{q}) + \beta\dot{q} \tag{4}$$

where F_c is the Coulomb friction coefficient, F_s is the static friction coefficient, $\dot{q}$ is the angular velocity, $\dot{q}_s$ is the maximum angular velocity under which the static friction exists, δ_s can be set to 2 [21], and β is the viscous friction coefficient.

In equation (4), $F_c, F_s, \dot{q}_s, \beta$ are the parameters to be calibrated. However, (4) can not be written in a linear form of $F_c, F_s, \dot{q}_s, \beta$. [7] neglected the nonlinear part of (4):

$$\boldsymbol{\tau}_f = \boldsymbol{F}_c\mathrm{sgn}(\dot{\boldsymbol{q}}) + \boldsymbol{\beta}\dot{\boldsymbol{q}}. \tag{5}$$

If the inertial force and static friction of the motors and gearboxes are ignored, the driving force $\boldsymbol{\tau}_j$ can be written as

$$\boldsymbol{\tau}_j = R\boldsymbol{\tau}_{total} - \boldsymbol{\tau}_f \tag{6}$$

where $\boldsymbol{R}$ is a diagonal matrix, R_{ii} is the reduction ratio of joint i, and $\boldsymbol{\tau}_{total}$ is the driving torque provided by the motor.

When the external forces are removed from the robot, $\boldsymbol{\tau}_{ext}$ is $\mathbf{0}$. Substitution of (3), (5), and (6) into (1) yields

$$\boldsymbol{R\tau}_{total} = \begin{bmatrix} \boldsymbol{A}_1 & \boldsymbol{A}_2 \end{bmatrix} \begin{bmatrix} \boldsymbol{X}_1 \\ \boldsymbol{X}_2 \end{bmatrix} = \boldsymbol{AX} \tag{7}$$

where

$$\begin{aligned} \boldsymbol{A}_1 &= \boldsymbol{K} \\ \boldsymbol{A}_2 &= \begin{bmatrix} \mathrm{sgn}(\dot{\boldsymbol{q}}) & \dot{\boldsymbol{q}} \end{bmatrix} \\ \boldsymbol{X}_1 &= \boldsymbol{\phi} \\ \boldsymbol{X}_2 &= \begin{bmatrix} \boldsymbol{F}_c \\ \boldsymbol{\beta} \end{bmatrix}. \end{aligned}$$

Some linear approximation methods [22] [23] have also been explored. The nonlinear part about static friction is replaced by some linear approximations to fit the friction curve. In [22], $\dot{\boldsymbol{q}}^{1/3}$ was introduced as an approximation:

$$\boldsymbol{\tau}_f = \boldsymbol{F}_c\mathrm{sgn}(\dot{\boldsymbol{q}}) + \boldsymbol{\beta}\dot{\boldsymbol{q}} + \boldsymbol{\gamma}\dot{\boldsymbol{q}}^{1/3}. \tag{8}$$

The inertial force of motors ($\boldsymbol{M}_j\dot{\boldsymbol{q}}$) are taken into consideration. Then (7) becomes

$$\boldsymbol{R\tau}_{total} = \begin{bmatrix} \boldsymbol{A}_1 & \boldsymbol{A}_2 & \boldsymbol{A}_3 \end{bmatrix} \begin{bmatrix} \boldsymbol{X}_1 \\ \boldsymbol{X}_2 \\ \boldsymbol{X}_3 \end{bmatrix} = \boldsymbol{AX} \tag{9}$$

where

$$\begin{aligned} \boldsymbol{A}_1 &= \boldsymbol{K} \\ \boldsymbol{A}_2 &= \begin{bmatrix} \mathrm{sgn}(\dot{\boldsymbol{q}}) & \dot{\boldsymbol{q}} & \dot{\boldsymbol{q}}^{1/3} \end{bmatrix} \\ \boldsymbol{A}_3 &= \ddot{\boldsymbol{q}} \\ \boldsymbol{X}_1 &= \boldsymbol{\phi} \\ \boldsymbol{X}_2 &= \begin{bmatrix} \boldsymbol{F}_c \\ \boldsymbol{\beta} \\ \boldsymbol{\gamma} \end{bmatrix} \\ \boldsymbol{X}_3 &= \boldsymbol{M}_j. \end{aligned}$$

A common solution of (7) and (9) is the pseudo-inverse method:

$$\hat{\boldsymbol{X}} = \boldsymbol{A}^{+}\boldsymbol{R\tau}_{total} \tag{10}$$

where $\hat{\boldsymbol{X}}$ is the estimate of $\boldsymbol{X}$.

However, owing to the measurement error and model approximation error, the estimated parameters are not accurate. The result obtained directly from the pseudo-inverse method may have a large deviation from the actual value. The same problem exists in the weighted pseudo-inverse method [24] and Kalman filter method [25]. Even worse, the inertia matrix may be non-positive and the mass may be minus. Thus, the parameters should be limited in the solution. A nonlinear optimal calibration method of the whole system is necessary in this case.

III. Sensorless Hand Guiding Control Scheme

A block diagram of the sensorless hand guiding control scheme is shown in Fig. 1. The industrial robot consists of the robot controller, servo system, motors, gearboxes, and manipulator links. The model of drive system includes the motors and gearboxes. It is built to estimate $\hat{\boldsymbol{\tau}}_j$. The model of links is built to estimate $\hat{\boldsymbol{\tau}}_d$. $\hat{\boldsymbol{\tau}}_{ext}$ is the subtraction of $\hat{\boldsymbol{\tau}}_j$ and $\hat{\boldsymbol{\tau}}_d$. Since the frequency of human operation is lower than that of the noise [6], $\hat{\boldsymbol{\tau}}_{ext}$ is filtered before the calculation of

This article has been accepted for publication in a future issue of this journal, but has not been fully edited. Content may change prior to final publication. Citation information: DOI 10.1109/TII.2019.2900119, IEEE Transactions on Industrial Informatics

$\hat{\boldsymbol{F}}_{ext}$. The force following controller generates the command trajectory based on the virtual mass and virtual friction model, which controls the robot to follow the external force.

A. Dynamic Model

1) Model of Drive:

The model of drive is built to analyze the inertial force and friction of the motor and gearbox. The vector of motor driving torque is defined as $\boldsymbol{\tau}_m$:

$$\boldsymbol{\tau}_m = \boldsymbol{\tau}_{total} - \boldsymbol{\tau}_{fm} - \boldsymbol{M}_m\boldsymbol{R}\ddot{\boldsymbol{q}} - \boldsymbol{\tau}_{\omega m} \tag{11}$$

where $\boldsymbol{\tau}_{total}$ is the total torque provided by the motor, $\boldsymbol{M}_m\boldsymbol{R}\ddot{\boldsymbol{q}}$ is the inertial force of the motor rotor, $\boldsymbol{M}_m$ is the rotational inertia of the motor rotor, $\boldsymbol{R}$ is the reduction ratio, $\boldsymbol{\tau}_{fm}$ is the motor friction, and $\boldsymbol{\tau}_{\omega m}$ is the motor disturbance.

The motor torque is output to the joint through the reducer:

$$\boldsymbol{\tau}_j = \boldsymbol{R}\boldsymbol{\tau}_m - \boldsymbol{\tau}_{fg} - \boldsymbol{M}_g\ddot{\boldsymbol{q}} - \boldsymbol{\tau}_{\omega g} \tag{12}$$

where $\boldsymbol{\tau}_j$ is the joint driving torque, $\boldsymbol{\tau}_{fg}$ is the reducer friction, $\boldsymbol{M}_g$ is the equivalent rotational inertia of reducer, and $\boldsymbol{\tau}_{\omega g}$ is the gearbox disturbance.

The joint friction $\boldsymbol{\tau}_f$ is

$$\boldsymbol{\tau}_f = \boldsymbol{R}\boldsymbol{\tau}_{fm} + \boldsymbol{\tau}_{fg}. \tag{13}$$

According to the LuGre friction model [21], $\boldsymbol{\tau}_{fm}$ and $\boldsymbol{\tau}_{fg}$ could be

$$\begin{aligned}
&\tau_{fmi} = \\
&\left[F_{cmii} + (F_{smii} - F_{cmii})e^{-\left|\frac{R_{ii}\dot{q}_i}{\dot{q}_{smi}}\right|^{\delta_s}}\right]\mathrm{sgn}(\dot{q}_i) + \beta_{mii}R_{ii}\dot{q}_i \\
&\tau_{fgi} = \left[F_{cgii} + (F_{sgii} - F_{cgii})e^{-\left|\frac{\dot{q}_i}{\dot{q}_{sgi}}\right|^{\delta_s}}\right]\mathrm{sgn}(\dot{q}_i) + \beta_{gii}\dot{q}_i
\end{aligned} \tag{14}$$

where the parameters in this equation have the same meaning as the parameters in (4).

Then the friction of joint i can be calculated as

$$\begin{aligned}
\tau_{fi} = {} & f_{1i}\mathrm{sgn}(\dot{q}_i) + f_{2i}e^{-\left|\frac{R_{ii}\dot{q}_i}{\dot{q}_{smi}}\right|^2}\mathrm{sgn}(\dot{q}_i) \\
& + f_{3i}e^{-\left|\frac{\dot{q}_i}{\dot{q}_{sgi}}\right|^2}\mathrm{sgn}(\dot{q}_i) + f_{4i}\dot{q}_i
\end{aligned} \tag{15}$$

where

$$\begin{aligned}
\tau_{fi} &= R_{ii}\tau_{fmi} + \tau_{fgi} \\
f_{1i} &= R_{ii}F_{cmii} + F_{cgii} \\
f_{2i} &= R_{ii}(F_{smii} - F_{cmii}) \\
f_{3i} &= F_{sgii} - F_{cgii} \\
f_{4i} &= R_{ii}\beta_{mii}R_{ii} + \beta_{gii}.
\end{aligned}$$

Substitution of (13) and (11) into (12) yields

$$\boldsymbol{\tau}_j = \boldsymbol{R}\boldsymbol{\tau}_{total} - \boldsymbol{\tau}_f - \boldsymbol{M}_j\ddot{\boldsymbol{q}} - \boldsymbol{\tau}_{\omega 1} \tag{16}$$

where

$$\begin{aligned}
\boldsymbol{M}_j &= \boldsymbol{R}\boldsymbol{M}_m\boldsymbol{R} + \boldsymbol{M}_g \\
\boldsymbol{\tau}_{\omega 1} &= (\boldsymbol{R}\boldsymbol{\tau}_{\omega m} + \boldsymbol{\tau}_{\omega g}).
\end{aligned}$$

The estimate of $\boldsymbol{\tau}_j$ is

$$\hat{\boldsymbol{\tau}}_j = \boldsymbol{\tau}_j + \boldsymbol{\tau}_{\omega 1}. \tag{17}$$

2) Model of Links:

The estimate of manipulator inertial force can be calculated from (2):

$$\hat{\boldsymbol{\tau}}_d = \hat{\boldsymbol{M}}(\boldsymbol{q})\ddot{\boldsymbol{q}} + \hat{\boldsymbol{V}}(\boldsymbol{q}, \dot{\boldsymbol{q}}) + \hat{\boldsymbol{G}}(\boldsymbol{q}) \tag{18}$$

where $\hat{\boldsymbol{\tau}}_d$, $\hat{\boldsymbol{M}}(\boldsymbol{q})$, $\hat{\boldsymbol{V}}(\boldsymbol{q}, \dot{\boldsymbol{q}})$, and $\hat{\boldsymbol{G}}(\boldsymbol{q})$ are the estimates of $\boldsymbol{\tau}_d$, $\hat{\boldsymbol{M}}(\boldsymbol{q})$, $\boldsymbol{V}(\boldsymbol{q}, \dot{\boldsymbol{q}})$, and $\boldsymbol{G}(\boldsymbol{q})$, respectively.

The relationship between $\boldsymbol{\tau}_d$ and $\hat{\boldsymbol{\tau}}_d$ is

$$\boldsymbol{\tau}_d = \hat{\boldsymbol{\tau}}_d + \boldsymbol{\tau}_{\omega 2} \tag{19}$$

where $\boldsymbol{\tau}_{\omega 2}$ is the modeling uncertainty.

3) Parameter Calibration:

The dynamic parameters, frictional parameters, and rotational inertial parameters need to be calibrated. The kinematic parameters and reduction ratios are supposed to be known. When calibrating, no external force is applied to the robot and $\boldsymbol{\tau}_{ext}$ is set to zero:

$$\boldsymbol{\tau}_{ext} = 0. \tag{20}$$

Substitution of (3), (16), (19), and (20) into (1) yields

$$\begin{aligned}
\boldsymbol{R}\boldsymbol{\tau}_{total} = {} & \boldsymbol{K}\boldsymbol{\phi} + \boldsymbol{f}_1\mathrm{sgn}(\dot{\boldsymbol{q}}) + \boldsymbol{f}_2e^{-\left|\frac{\boldsymbol{R}\dot{\boldsymbol{q}}}{\dot{\boldsymbol{q}}_{sm}}\right|^2}\mathrm{sgn}(\dot{\boldsymbol{q}}) \\
& + \boldsymbol{f}_3e^{-\left|\frac{\dot{\boldsymbol{q}}}{\dot{\boldsymbol{q}}_{sg}}\right|^2}\mathrm{sgn}(\dot{\boldsymbol{q}}) + \boldsymbol{f}_4\dot{\boldsymbol{q}} + \boldsymbol{M}_j\ddot{\boldsymbol{q}} + \boldsymbol{\tau}_\omega
\end{aligned} \tag{21}$$

where $\boldsymbol{\tau}_\omega = \boldsymbol{\tau}_{\omega 1} + \boldsymbol{\tau}_{\omega 2}$. $\boldsymbol{\tau}_\omega$ represents the modeling uncertainties and measurement noises.

Here $\boldsymbol{\phi}$, $\boldsymbol{f}_1$, $\boldsymbol{f}_2$, $\dot{\boldsymbol{q}}_{sm}$, $\boldsymbol{f}_3$, $\dot{\boldsymbol{q}}_{sg}$, $\boldsymbol{f}_4$, and $\boldsymbol{M}_j$ are the parameters to be calibrated. Define the set of the parameters as

$$\boldsymbol{X} = \{\boldsymbol{\phi}, \boldsymbol{f}_1, \boldsymbol{f}_2, \dot{\boldsymbol{q}}_{sm}, \boldsymbol{f}_3, \dot{\boldsymbol{q}}_{sg}, \boldsymbol{f}_4, \boldsymbol{M}_j\}. \tag{22}$$

An optimization method is used to calibrate the parameters. The steps are as follows.

Step 1 The initial dynamic parameters ($\boldsymbol{\phi}_{init}$) are calculated from the robot's three-dimensional model.

Step 2 The parameters that have no effect on the dynamic model are set to initial values in $\boldsymbol{\phi}_{init}$. The base inertial parameters [26] are determined by the structure of the manipulator. The other parameters are set around $\boldsymbol{\phi}_{init}$, allowing a certain range of error.

Step 3 Set the ranges of the friction and motor inertial parameters: $\boldsymbol{f}_1$, $\boldsymbol{f}_2$, $\dot{\boldsymbol{q}}_{sm}$, $\boldsymbol{f}_3$, $\dot{\boldsymbol{q}}_{sg}$, $\boldsymbol{f}_4$, and $\boldsymbol{M}_j$.

$$\begin{aligned}
&(\boldsymbol{f}_1)_{ii} > 0 \\
&(\boldsymbol{f}_2)_{ii} > 0 \\
&0 < (\dot{\boldsymbol{q}}_{sm})_i < \max((\dot{\boldsymbol{q}}_{sm})_i) \\
&(\boldsymbol{f}_3)_{ii} > 0 \\
&0 < (\dot{\boldsymbol{q}}_{sg})_i < \max((\dot{\boldsymbol{q}}_{sg})_i) \\
&(\boldsymbol{f}_4)_{ii} > 0
\end{aligned} \tag{23}$$

$$(\boldsymbol{M}_j)_{ii} = 0 \tag{24}$$

where $\max((\dot{\boldsymbol{q}}_{sm})_i)$ and $\max((\dot{\boldsymbol{q}}_{sg})_i)$ are the maximum angular velocity under which the static friction exists.

Step 4 Obtain the values of $\boldsymbol{\tau}_{total}$ and $\boldsymbol{q}$ with an optimal trajectory [2] without external forces and calculate the vector $R\boldsymbol{\tau}_{total}$.

Step 5 Add the constraints that the inertia matrices $\bar{\boldsymbol{I}}_i$ in (3) are positive-definite.

This article has been accepted for publication in a future issue of this journal, but has not been fully edited. Content may change prior to final publication. Citation information: DOI 10.1109/TII.2019.2900119, IEEE Transactions on Industrial Informatics

Step 6 The noise $\boldsymbol{\tau}_\omega$ is

$$\begin{aligned}\boldsymbol{\tau}_\omega = \\ \boldsymbol{R}\boldsymbol{\tau}_{total} - \Big[\boldsymbol{K}\boldsymbol{\phi} + \boldsymbol{f}_1\mathrm{sgn}(\dot{\boldsymbol{q}}) + \boldsymbol{f}_2 e^{-\left|\frac{\boldsymbol{R}\dot{\boldsymbol{q}}}{\dot{q}_{sm}}\right|^2}\mathrm{sgn}(\dot{\boldsymbol{q}}) \\ + \boldsymbol{f}_3 e^{-\left|\frac{\dot{\boldsymbol{q}}}{\dot{q}_{sg}}\right|^2}\mathrm{sgn}(\dot{\boldsymbol{q}}) + \boldsymbol{f}_4\dot{\boldsymbol{q}} + \boldsymbol{M}_j\ddot{\boldsymbol{q}}\Big].\end{aligned} \tag{25}$$

Define the optimization target as the sum of the mean and standard deviation of the noise $\boldsymbol{\tau}_\omega$:

$$\hat{\boldsymbol{X}} = \{\boldsymbol{X}|\min(J = \sum_{i=1}^{n}|\bar{\tau}_{\omega i}| + K_\omega\sum_{i=1}^{n}\sigma(\tau_{\omega i}))\} \tag{26}$$

where $\bar{\boldsymbol{\tau}}_{\omega i}$ is the mean of $\boldsymbol{\tau}_{\omega i}$, and $K_\omega \in \Re^1$ is a positive balance between the mean and standard deviation.

Step 7 Solve the optimization problem.

The particle filter algorithm [27] is used to solve the optimization problem here. After the iterative calculation of the sampled trajectory, the parameters are calibrated.

B. Guiding Control Based on Virtual Mass and Virtual Friction

The external force in joint space can be calculated as follows:

$$\boldsymbol{\tau}_{ext} = \hat{\boldsymbol{\tau}}_d - \hat{\boldsymbol{\tau}}_j + \boldsymbol{\tau}_\omega. \tag{27}$$

The noise $\boldsymbol{\tau}_\omega$ exists in the calculation owing to the accuracy of the model and the interference of the gearbox. The relationship between the external force in Cartesian space and the joint torque can be described as

$$\hat{\boldsymbol{\tau}}_d - \hat{\boldsymbol{\tau}}_j = {\boldsymbol{J}_b}^T\hat{\boldsymbol{F}}_{ext} \tag{28}$$

where $\boldsymbol{J}_b$ is the Jacobian matrix and $\hat{\boldsymbol{F}}_{ext}$ is the estimated external force: $\boldsymbol{F}_{ext} = [\ \tau_x \quad \tau_y \quad \tau_z \quad F_x \quad F_y \quad F_z\ ]^T$.

Substitution of (27) into (26) yields

$$\boldsymbol{\tau}_{ext} = {\boldsymbol{J}_b}^T\hat{\boldsymbol{F}}_{ext} + \boldsymbol{\tau}_\omega. \tag{29}$$

A low-pass filter is used to limit the high-frequency part of the noise. The calculation of $\hat{\boldsymbol{F}}_{ext}$ is

$$\hat{\boldsymbol{F}}_{ext} = {\boldsymbol{J}_b}^{-T}\cdot Filter(\boldsymbol{\tau}_{ext} - \boldsymbol{\tau}_\omega). \tag{30}$$

With the calculated external force $\hat{\boldsymbol{F}}_{ext}$, it is possible to control the robot to follow the guiding hand. A strategy is to set a virtual mass $\boldsymbol{M}_k$ and a virtual friction $\boldsymbol{F}_{fk}$ for the end-effector. When external force $\hat{\boldsymbol{F}}_{ext}$ is applied, the end-effector overcomes the virtual friction $\boldsymbol{F}_{fk}$ and moves along the direction of $\hat{\boldsymbol{F}}_{ext}$. The acceleration in Cartesian space is defined as $\boldsymbol{a}_k$. The motion satisfies

$$\hat{\boldsymbol{F}}_{ext} + \boldsymbol{F}_{fk} = \boldsymbol{M}_k\boldsymbol{a}_k \tag{31}$$

where $\boldsymbol{a}_k \in \Re^{6\times1}$ is a six-dimensional vector defined as $\boldsymbol{a}_k = [\ \alpha_x \quad \alpha_y \quad \alpha_z \quad a_x \quad a_y \quad a_z\ ]^T$. $\boldsymbol{M}_k \in \Re^{6\times6}$ is defined as

$$\boldsymbol{M}_k = \begin{bmatrix}\boldsymbol{I}_{k3} & 0\\ 0 & \boldsymbol{M}_{k3}\end{bmatrix}$$

$$\boldsymbol{I}_{k3} = \begin{bmatrix}I_{kxx} & 0 & 0\\ 0 & I_{kyy} & 0\\ 0 & 0 & I_{kzz}\end{bmatrix}$$

$$\boldsymbol{M}_{k3} = \begin{bmatrix}M_{kx} & 0 & 0\\ 0 & M_{ky} & 0\\ 0 & 0 & M_{kz}\end{bmatrix}$$

where $I_{kxx}, I_{kyy}, I_{kzz}$ are the virtual inertias and M_{kx}, M_{ky}, M_{kz} are the virtual masses. They can be changed according to the guiding performance and safety requirements.

The direction of virtual friction $\boldsymbol{F}_{fk}$ is always opposite to the direction of velocity. For a simple guiding experience, $\boldsymbol{F}_{fk}$ can be set to

$$(F_{fk})_i = \begin{cases}-\delta_i, & V_i > 0\\ 0, & V_i = 0\\ \delta_i, & V_i < 0\end{cases} \tag{32}$$

where $\delta_i > 0$.

Then, the trajectory in Cartesian space is obtained by

$$(a_k)_i = \begin{cases}M_{kii}^{-1}\left[(\hat{F}_{ext})_i + (F_{fk})_i\right], (\hat{F}_{ext})_i \geq \delta_i\\ M_{kii}^{-1}(F_{fk})_i, -\delta_i < (\hat{F}_{ext})_i < \delta_i, V_{ki} \neq 0\\ 0, -\delta_i < (\hat{F}_{ext})_i < \delta_i, V_{ki} = 0\\ M_{kii}^{-1}\left[(\hat{F}_{ext})_i + (F_{fx})_i\right], (\hat{F}_{ext})_i \leq -\delta_i\end{cases}. \tag{33}$$

The velocity $\boldsymbol{v}_k$ and position $\boldsymbol{p}_k$ are obtained by integrating the acceleration $\boldsymbol{a}_k$. The command angular position, angular velocity, and angular acceleration $\boldsymbol{q}_c, \dot{\boldsymbol{q}}_c, \ddot{\boldsymbol{q}}_c$ are calculated in the robot controller and sent to the driving system. Then the robot end-effector moves following the guiding hand.

Remark: The magnitude of noise $\boldsymbol{\tau}_\omega$ depends on the accuracy of parameters in (22). It changes with the angular position, angular velocity, and angular acceleration. The noise affects the velocity by

$$\boldsymbol{M}_k\Delta\boldsymbol{V}_k = \int_0^T {\boldsymbol{J}_b}^{-T}\cdot Filter(\boldsymbol{\tau}_\omega)dt \doteq {\boldsymbol{J}_b}^{-T}\bar{\boldsymbol{\tau}}_\omega T \tag{34}$$

where $\bar{\boldsymbol{\tau}}_\omega$ is the mean of $\boldsymbol{\tau}_\omega$.

If the mean of the noise is close to zero and the standard deviation is small, the velocity is less affected by $\boldsymbol{\tau}_\omega$. Thus, the optimization target in (26) is set to the sum of the mean and standard deviation. Moreover, the low-pass filter helps to reduce the noise in joint torque and leads to a better guiding performance.

The friction adds a certain amount of resistance to make the velocity less disturbing. However, a large virtual friction makes it hard to guide the robot. Therefore, the friction can be set separately according to the robot state. When guiding the robot, the friction is set small. The noise and friction affect the velocity by

$$\boldsymbol{M_k}\Delta\boldsymbol{V_k} \doteq {\boldsymbol{J}_b}^{-T}\bar{\boldsymbol{\tau}}_\omega T + \boldsymbol{F}_{fk}T. \tag{35}$$

To produce a resistance feel similar to push a box on the ground, the friction should be larger than the noise:

$$|F_{fki}| = r\left|{\boldsymbol{J}_b}^{-T}\bar{\boldsymbol{\tau}}_\omega\right|_i, r \geq 1. \tag{36}$$

This article has been accepted for publication in a future issue of this journal, but has not been fully edited. Content may change prior to final publication. Citation information: DOI 10.1109/TII.2019.2900119, IEEE Transactions on Industrial Informatics

When the external force is removed, the friction could be set larger instead. The range of r in (36) can be set to $r \geq 3$.

IV. Experiments and Discussions

A six-degree-of-freedom industrial robot Efort ER20-C10 is used in the experiments. The maximum payload of the robot is 20kg and the operating radius is about 1.7m. The robot controller is a Beckhoff industrial computer CX5130. The cycle of the force following controller is 10ms and the cycle of the robot controller is 1ms. The servo drivers are Sanmotion AC servos, which can feed back the current value to the controller. The controller and servo drivers are connected by EtherCAT. All six joints are rotary joints with reducers. No force sensors are installed. The control system and D-H frames are shown in Fig. 2. The reduction ratio, maximum torque, and power of each joint are listed in Table I.

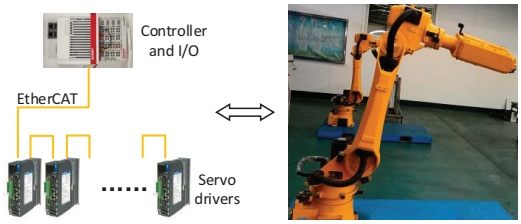

(a) The control system with EtherCAT

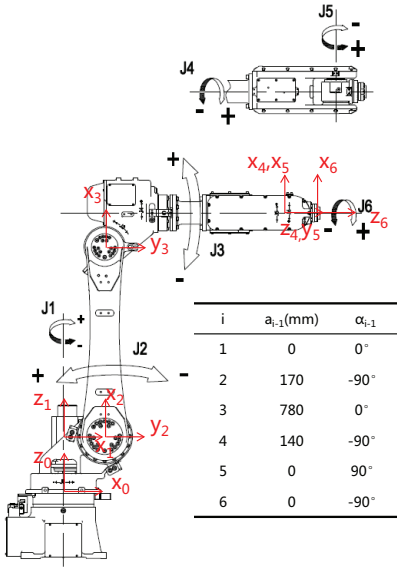

i	a_{i-1}(mm)	α_{i-1}	d_i(mm)	θ_i
1	0	0°	293.6	0°
2	170	-90°	0	-90°
3	780	0°	0	0°
4	140	-90°	760	0°
5	0	90°	0	0°
6	0	-90°	103	0°

(b) The D-H frames and table

Fig. 2. Efort ER20-C10 robot system

The experiments include two parts: parameter calibration and guiding movement. The procedures and results will be described respectively.

A. Experiments of Parameter Calibration

In the calibration, no external force is applied to the robot. Trajectory points consist of $\boldsymbol{\tau}_{total}$ and $\boldsymbol{q}$ are sampled from an optimal trajectory. Since the static friction is difficult to estimate when standing still, these points are filtered out. Then, the points are input into the optimization solver for calculation. The parameters in (22) are to be calibrated. The three-dimensional robot model provided by the official site is not accurate enough, so the parameter ranges are set to $\pm 30\%$ around the initial values.

$$\begin{aligned} &m_i \in m_i \pm m_i \cdot 30\% \\ &\boldsymbol{c_i} \in \boldsymbol{c}_i \pm max(abs(\boldsymbol{c}_{ia})) \cdot 30\%, a = 1,2,3 \\ &\bar{\boldsymbol{I}}_i \in \bar{\boldsymbol{I}}_i \pm max(abs(\bar{\boldsymbol{I}}_{iab})) \cdot 30\%, a = 1..6, b = 1..6. \end{aligned} \tag{37}$$

The friction parameters $\boldsymbol{f}_1$, $\boldsymbol{f}_2$, $\boldsymbol{f}_3$, and $\boldsymbol{f}_4$ are difficult to estimate. The ranges of these parameters are set large enough for calibration. The K_ω in (26) is set to 1.

The calibration result is shown in Fig. 3. Six figures show the results of six joints. $\boldsymbol{R}\boldsymbol{\tau}_{total}$ is calculated from the motor current and drawn as "Calculated torque" in black lines. $\boldsymbol{K}\boldsymbol{\phi} + \boldsymbol{\tau}_f + \boldsymbol{M}_j\ddot{\boldsymbol{q}}$ is calculated with the calibrated parameters and drawn as "Proposed method" in red dash-dot lines. It can be seen that the two torques almost match each other. The means and standard deviations of $\boldsymbol{\tau}_\omega$ are calculated by (25) and listed in Table II. The means and standard deviations are small. Thus, the virtual friction can be set small, which is good for the guiding performance.

The result is compared with two other models described in [7] and [22]. Parameters are calculated by the pseudo-inverse method in (10). The means and standard deviations are calculated and listed in Table II. The calibrated torques are drawn in blue dashed lines and green dotted lines in Fig. 3.

Comparing the results, it can be seen that J of the two models are larger than that of the model presented in this paper. The models in [7] and [22] do not calculate the torques of the driving system accurately and cause larger errors of J. Although the calculation of the linear models is relatively simple, the pseudo-inverse method is a curve fitting method. The deviations between the parameters and the true values are large.

B. Experiments of Guiding Movement

The calibrated parameters are used for guiding movement in this section. To test the accuracy of external force estimator, payloads of different weights are installed on the end-effector. The external force estimated by (30) and the weight of payload are listed in Table III. The payload is estimated during moving and the inertial force of payload is considered.

As can be seen in Table III, the accuracy of estimation is smaller than 10N. In fact, the error approaches zero with the number of iterations. Owing to the modeling uncertainties and measurement noises, it is not as accurate as force sensors, but enough for guiding the robot.

To move the robot, the virtual mass and virtual friction parameters are set. For safety reasons, the maximum velocity is set to $0.2rad/s$ and $0.2m/s$. The minimum acceleration time is set to $0.5s$. Thus, the maximum acceleration is set to $0.4rad/s^2$ and $0.4m/s^2$ (0.4=0.2/0.5). Assuming the external force of $100Nm$ or $100N$ produces an acceleration of $0.1rad/s^2$ or $0.1m/s^2$, the virtual mass should be $1000kg \cdot m^2$ or $1000kg$ (1000=100/0.1). Considering the error of $\hat{\boldsymbol{F}}_{ext}$, the

This article has been accepted for publication in a future issue of this journal, but has not been fully edited. Content may change prior to final publication. Citation information: DOI 10.1109/TII.2019.2900119, IEEE Transactions on Industrial Informatics

TABLE I
THE REDUCTION RATIO, MAX TORQUE AND POWER OF EACH JOINT

Item	$Joint1$	$Joint2$	$Joint3$	$Joint4$	$Joint5$	$Joint6$
Ratio	147	178	164	77	80	50
Max Torque(Nm)	1764	2138	418	105	109	35
Power(w)	2000	2000	750	400	200	200

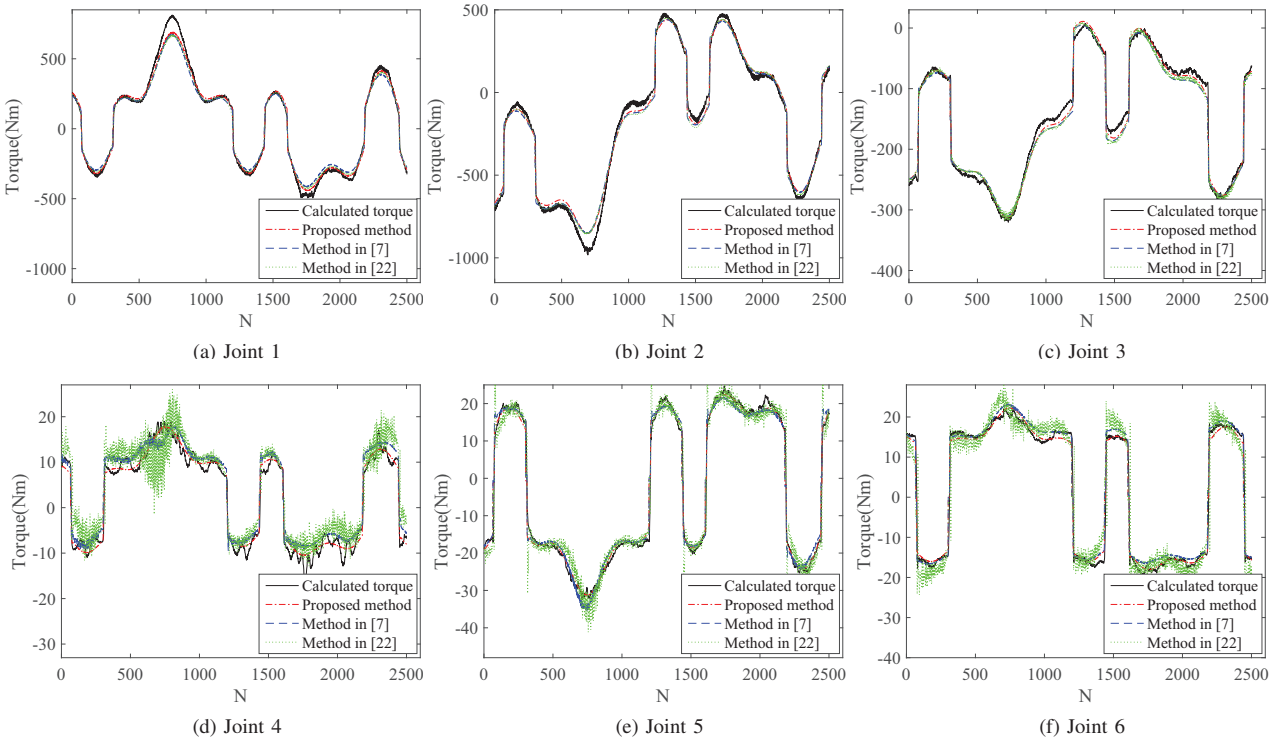

(a) Joint 1 (b) Joint 2 (c) Joint 3

(d) Joint 4 (e) Joint 5 (f) Joint 6

Fig. 3. Comparisons between the torques calculated from the motor currents and the torques calculated by different methods (proposed method, method in [7] and method in [22])

TABLE II
THE RESULTS OF DIFFERENT CALIBRATION METHODS

Item	Method in [7]		Method in [22]		Proposed method	
	Mean(Nm)	Std/Max Torque	Mean(Nm)	Std/Max Torque	Mean(Nm)	Std/Max Torque
Joint1	-8.49	2.59%	-4.52	2.21%	-4.52	1.84%
Joint2	3.76	1.86%	2.44	1.80%	-4.06	1.71%
Joint3	6.34	2.80%	5.56	2.77%	2.35	2.50%
Joint4	-1.69	1.89%	-2.34	3.37%	-0.109	1.60%
Joint5	0.0623	2.19%	0.0965	3.38%	0.0755	1.86%
Joint6	-0.925	5.92%	0.230	11.5%	-0.0261	5.67%
$J = \sum_{i=1}^{n} \lvert\bar{\tau}_{\omega i}\rvert + K_\omega \sum_{i=1}^{n} \sigma(\tau_{\omega i})$	124.85		115.47		96.36	

virtual friction is set to 15Nm/15N and the stopping friction is set larger. The parameters can be changed according to the guiding performance.

During the guiding movement, the robot follows the external force from one pose to another. An example of the external force and velocity is shown in Fig. 4. The torques/forces are drawn in green solid lines and the velocities are drawn in red dashed lines. When N is smaller than 200, no external force is applied. Owing to the estimation error, $\hat{\boldsymbol{F}}_{ext}$ is not $\mathbf{0}$. However, the command velocity is $\mathbf{0}$. Then, the external force is applied and the end-effector starts to move in directions (v_x and v_z) where the external force is larger than 15Nm/15N. Finally, the external force is removed, and the end-effector decelerates until stopped under the effect of stopping friction (50Nm/50N).

The result is compared with the closed-loop velocity control

This article has been accepted for publication in a future issue of this journal, but has not been fully edited. Content may change prior to final publication. Citation information: DOI 10.1109/TII.2019.2900119, IEEE Transactions on Industrial Informatics

TABLE III
THE ESTIMATED EXTERNAL FORCE AND THE WEIGHT OF PAYLOAD

Item	Payload1	Payload2	Payload3	Payload4
Payload(N)	71.54	101.92	120.54	154.84
Estimated Result(N)	66.74	102.80	113.68	147.00

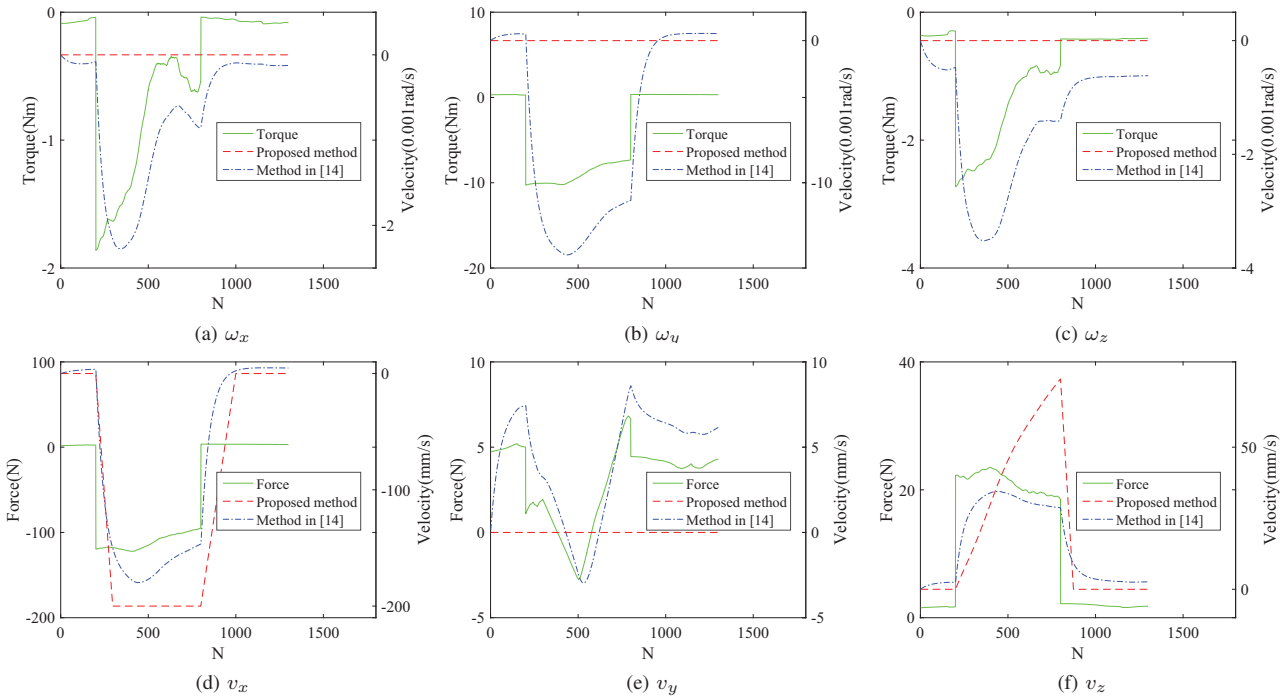

Fig. 4. The external force and velocity.

TABLE IV
THE VIRTUAL MASS AND VIRTUAL FRICTION PARAMETERS

Item	ω_x	ω_y	ω_z	x	y	z
Mass	$1000(kg \cdot m^2)$	$1000(kg \cdot m^2)$	$1000(kg \cdot m^2)$	$1000(kg)$	$1000(kg)$	$1000(kg)$
Friction	$15(Nm)$	$15(Nm)$	$15(Nm)$	$15(N)$	$15(N)$	$15(N)$
Stopping friction	$50(Nm)$	$50(Nm)$	$50(Nm)$	$50(N)$	$50(N)$	$50(N)$

strategy [6] [14]. The velocity of this method is drawn as "Method in [14]" in Fig. 4 with blue dash-dot lines. The following conclusions can be drawn.

1 The robot moves slowly when no external force is applied. The stopping velocity has a gradual approaching process when the external force is removed. While the method in this paper does not have these problems. The estimation error of external force has no influence on the velocity.
2 It is difficult to move the robot in a certain direction. There are noises in other directions. In the method in this paper, v_x and v_z are not zeroes, while velocities of the other directions keep stationary.

The external forces in Cartesian space and generated trajectory are shown in Fig. 5. The blue arrows are the external forces and the red line is the generated trajectory of the end-effector. The length of the arrow is proportional to the magnitude of external force. It can be seen that the end-effector moves along the main direction of external force. The limitations in acceleration and velocity cause direction deviations between the arrow and trajectory. When the external force is removed, the end-effector stops and keeps still.

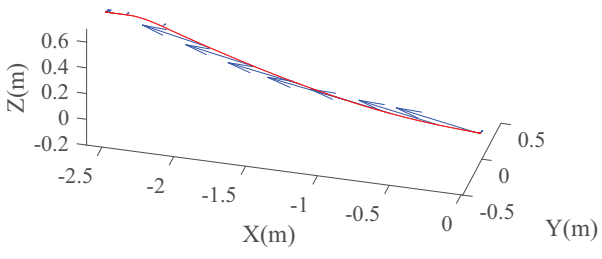

Fig. 5. The external force and generated trajectory in Cartesian space (blue arrows: forces, red: trajectory)

This article has been accepted for publication in a future issue of this journal, but has not been fully edited. Content may change prior to final publication. Citation information: DOI 10.1109/TII.2019.2900119, IEEE Transactions on Industrial Informatics

Finally, the proposed method is used to generate a trajectory for a welding task. In Fig. 6(a), the welding seam of an aluminum radiator is shown, which requires to be followed by the end-effector. First, the end-effector is guided to the start point P_1. It is then guided along the welding seam to end point P_2. In Fig 6(b), the guiding trajectory is sampled and drawn with discrete points. The solid line connecting point P_1 and P_2 generates the final welding trajectory. Finally, the robot can use this trajectory for welding between point P_1 and P_2.

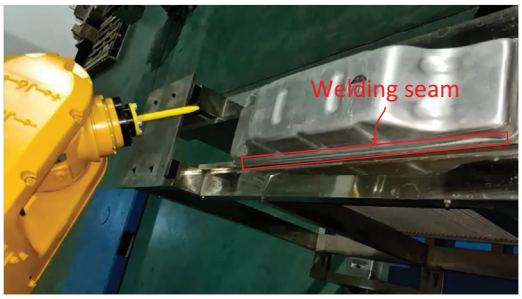

(a) The aluminum radiator for welding

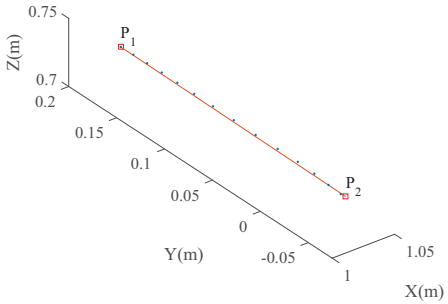

(b) The guiding trajectory and the generated welding trajectory

Fig. 6. A welding trajectory generated by hand guiding

V. Conclusion

This paper has proposed a sensorless hand guiding scheme with an external force estimator and a force following controller for the industrial robot teaching. A nonlinear model of the driving system and manipulator links is presented for the external force estimator. The model parameters are calibrated based on particle filter algorithm under some reasonable constraints. Compared with two classic models, the proposed model improves the accuracy of external force estimation. Then the virtual mass and virtual friction are presented and used in the force following controller design for making the robot easier to guide by hand. The experimental results show the proposed control scheme not only makes the end-effector of a six-degree-of-freedom industrial manipulator follow the direction of external force but also suppresses jitters. And the sensorless hand guiding scheme is also applicable to other industrial robots.

References

[1] P. M. Kebria, S. Al-Wais, H. Abdi, and S. Nahavandi, "Kinematic and dynamic modelling of ur5 manipulator," in *2016 IEEE Int. Conf. Syst., Man, Cybern. (SMC)*, Oct. 2016, pp. 004 229–004 234.

[2] Y. R. Stürz, L. M. Affolter, and R. S. Smith, "Parameter identification of the kuka lbr iiwa robot including constraints on physical feasibility," *IFAC-PapersOnLine*, vol. 50, no. 1, pp. 6863–6868, Jul. 2017. [Online]. Available: http://linkinghub.elsevier.com/retrieve/pii/S2405896317317147

[3] A. Cirillo, F. Ficuciello, C. Natale, S. Pirozzi, and L. Villani, "A conformable force/tactile skin for physical human-robot interaction," *IEEE Robot. Autom. Lett.*, vol. 1, no. 1, pp. 41–48, Jan. 2016.

[4] Y. Sun, Y. Liu, and H. Liu, "Analysis calibration system error of six-dimension force/torque sensor for space robot," in *2014 IEEE Int. Conf. Mechatron. Autom.*, Aug. 2014, pp. 347–352.

[5] A. de Luca and R. Mattone, "Sensorless robot collision detection and hybrid force/motion control," in *Proc. IEEE Int. Conf. Robot. Autom.*, Apr. 2005, pp. 999–1004.

[6] M. S. Erden and T. Tomiyama, "Human-intent detection and physically interactive control of a robot without force sensors," *IEEE Trans. Robot.*, vol. 26, no. 2, pp. 370–382, Apr. 2010.

[7] D. Wu, Q. Liu, W. Xu, A. Liu, Z. Zhou, and D. T. Pham, "External force detection for physical human-robot interaction using dynamic model identification," in *Int. Conf. Intell. Robot. Appl.*, ser. Lecture Notes in Computer Pullishing, Y. Huang, H. Wu, H. Liu, and Z. Yin, Eds., vol. 10462. Cham: Springer International Publishing, 2017, pp. 581–592. [Online]. Available: http://link.springer.com/10.1007/978-3-319-65289-4_55

[8] B. Yao, Z. Zhou, L. Wang, W. Xu, Q. Liu, and A. Liu, "Sensorless and adaptive admittance control of industrial robot in physical human-robot interaction," *Robot. Comput.-Integr. Manuf.*, vol. 51, pp. 158 – 168, Jun. 2018. [Online]. Available: http://www.sciencedirect.com/science/article/pii/S0736584517301564

[9] M. Brunot, A. Janot, P. Young, and F. Carrillo, "An improved instrumental variable method for industrial robot model identification," *Control Eng. Practice*, vol. 74, pp. 107 – 117, 2018. [Online]. Available: http://www.sciencedirect.com/science/article/pii/S0967066118300261

[10] M. Gautier, A. Janot, and P. Vandanjon, "A new closed-loop output error method for parameter identification of robot dynamics," *IEEE Trans Control Syst Technol*, pp. 428–444, 2013.

[11] Y. Nagamatsu, T. Shirai, H. Suzuki, Y. Kakiuchi, K. Okada, and M. Inaba, "Distributed torque estimation toward low-latency variable stiffness control for gear-driven torque sensorless humanoid," in *2017 IEEE/RSJ Int. Conf. Intell. Robot. Syst. (IROS)*, Sep. 2017, pp. 5239–5244.

[12] M. Yuan, Z. Chen, B. Yao, and J. Hu, "A general online trajectory planning framework in the case of desired function unknown in advance," *IEEE Trans. Ind. Informat.*, pp. 1–1, Sep. 2018.

[13] Z. Chen, Y. Pan, and J. Gu, "Integrated adaptive robust control for multilateral teleoperation systems under arbitrary time delays," *Int. J. Robust Nonlinear Control*, vol. 26, no. 12, pp. 2708–2728, 2016.

[14] S. D. Lee, K. H. Ahn, and J. B. Song, "Torque control based sensorless hand guiding for direct robot teaching," in *2016 IEEE/RSJ Int. Conf. Intell. Robot. Syst. (IROS)*, Oct. 2016, pp. 745–750.

[15] C. Gosselin, T. Laliberte, B. Mayer-St-Onge, S. Foucault, A. Lecours, V. Duchaine, N. Paradis, D. Gao, and R. Menassa, "A friendly beast of burden: A human-assistive robot for handling large payloads," *IEEE Robot. Autom. Mag.*, vol. 20, no. 4, pp. 139–147, Dec. 2013.

[16] M. Sharifi, S. Behzadipour, and G. Vossoughi, "Nonlinear model reference adaptive impedance control for human-robot interactions," *Control Eng. Practice*, vol. 32, pp. 9 – 27, Nov. 2014. [Online]. Available: http://www.sciencedirect.com/science/article/pii/S0967066114001713

[17] A. Calanca, L. Capisani, and P. Fiorini, "Robust force control of series elastic actuators," *Actuators*, vol. 3, no. 3, pp. 182–204, Jul. 2014.

[18] V. Duchaine and C. M. Gosselin, "General model of human-robot cooperation using a novel velocity based variable impedance control," in *2nd Jt. EuroHaptics Conf. Symp. Haptic Interfaces for Virtual Env. Teleoper. Syst. (WHC'07)*, Mar. 2007, pp. 446–451.

[19] C. Yang, H. Ma, and M. Fu, *Robot Kinematics and Dynamics Modeling*. Singapore: Springer Singapore, 2016, pp. 27–48.

[20] J. Hollerbach, W. Khalil, and M. Gautier, "Model identification," in *Springer Handbook of Robotics*. Springer Berlin Heidelberg, 2016, ch. chapter 6, pp. 113–138.

[21] B. Bona and M. Indri, "Friction compensation in robotics: an overview," in *Proc. 44th IEEE Conf. Decis. Control*, Dec. 2005, pp. 4360–4367.

This article has been accepted for publication in a future issue of this journal, but has not been fully edited. Content may change prior to final publication. Citation information: DOI 10.1109/TII.2019.2900119, IEEE Transactions on Industrial Informatics

[22] M. Grotjahn, M. Daemi, and B. Heimann, "Friction and rigid body identification of robot dynamics," *Int. J. Solids Struct.*, vol. 38, no. 10-13, pp. 1889–1902, Mar. 2001. [Online]. Available: http://linkinghub.elsevier.com/retrieve/pii/S0020768300001414

[23] N. Kammerer and P. Garrec, "Dry friction modeling in dynamic identification for robot manipulators: Theory and experiments," in *2013 IEEE Int. Conf. Mechatron. (ICM)*, Feb. 2013, pp. 422–429.

[24] A. Wahrburg, J. Bös, K. D. Listmann, F. Dai, B. Matthias, and H. Ding, "Motor-current-based estimation of cartesian contact forces and torques for robotic manipulators and its application to force control," *IEEE Trans. Autom. Sci. Eng.*, vol. 15, no. 2, pp. 879–886, Apr. 2018.

[25] M. Van Damme, P. Beyl, B. Vanderborght, V. Grosu, R. Van Ham, I. Vanderniepen, A. Matthys, and D. Lefeber, "Estimating robot end-effector force from noisy actuator torque measurements," in *IEEE Int. Conf. Robot. Autom.*, May. 2011, pp. 1108–1113. [Online]. Available: http://ieeexplore.ieee.org/document/5980210/

[26] W. Khalil and E. Dombre, "Dynamic modeling of serial robots," in *Modeling, Identification and Control of Robots*. Oxford: Butterworth-Heinemann, 2002, pp. 191–233. [Online]. Available: http://www.sciencedirect.com/science/article/pii/B9781903996669500270

[27] J. V. Candy, *Bayesian signal processing: classical, modern, and particle filtering methods*. John Wiley & Sons, Inc., Jul. 2016, vol. 54.

Shaolin Zhang received the B.E. and M.E. degrees in mechanical science and engineering from Huazhong University of Science and Technology, Wuhan, China, in 2010 and 2013, respectively. He is currently working toward the Ph.D. degree in the Institute of Automation, Chinese Academy of Science, Beijing, China. His current research interests include intelligent robot system and automation systems.

Shuo Wang received the B.E. degree in electrical engineering from the Shenyang Architecture and Civil Engineering Institute, Shenyang, China, the M.E. degree in industrial automation from the Northeastern University, Shenyang, and the Ph.D. degree in control theory and control engineering from the Institute of Automation, Chinese Academy of Sciences, Beijing, China, in 1995, 1998 and 2001, respectively. He is currently a Professor in the State Key Laboratory of Management and Control for Complex Systems, Institute of Automation, Chinese Academy of Sciences, Beijing, China. His research interests include biomimetic robot, underwater robot, and multirobot systems.

Fengshui Jing was born in Shandong Province, China, on January 22, 1969. He received the B.E. degree in mining engineering from Huainan Mining Institute, Anhui Province, China, in 1991 and the M.S. degree in safety technology and engineering from Shandong Mining Institute, Shandong Province, in 1994. In 2002, he received the Ph.D. degree in control theory and control engineering from the Institute of Automation, Chinese Academy of Sciences, Beijing, China. From 1994 to 1999, he was an Assistant Professor at the Mechanical and Electrical Engineering Department, Shandong Agricultural University, Shandong Province. He is currently a Professor in the State Key Laboratory of Management and Control for Complex Systems, Institute of Automation, Chinese Academy of Sciences, Beijing, China. His areas of interests include robotics, computer vision, and manufacturing systems.

Min Tan received the B.E. degree in control engineering from Tsinghua University, Beijing, China, and the Ph.D. degree in control theory and control engineering from the Institute of Automation, Chinese Academy of Sciences, Beijing, in 1986 and 1990, respectively. He is currently a Professor in the State Key Laboratory of Management and Control for Complex Systems, Institute of Automation, Chinese Academy of Sciences. His research interests include advanced robot control, biomimetic robot, multirobot system.